View metadata, citation and similar papers at core.ac.uk

brought to you by CORE

provided by University of Bath Research Portal

Citation for published version:
Walsh, D, Sanchez-Ballester, NM, Ting, VP, Hall, SR, Terry, LR & Weller, MT 2015, 'Visible light promoted photocatalytic water oxidation: effect of metal oxide catalyst composition and light intensity', Catalysis Science and Technology, vol. 5, no. 10, pp. 4760-4764. https://doi.org/10.1039/C5CY01203A

DOI:
10.1039/C5CY01203A

Publication date:
2015

Document Version
Peer reviewed version

Link to publication

University of Bath

General rights
Copyright and moral rights for the publications made accessible in the public portal are retained by the authors and/or other copyright owners and it is a condition of accessing publications that users recognise and abide by the legal requirements associated with these rights.

Take down policy
If you believe that this document breaches copyright please contact us providing details, and we will remove access to the work immediately and investigate your claim.

Download date: 13. May. 2019

Visible light promoted photocatalytic water oxidation: effect of metal oxide catalyst composition and light intensity

Dominic Walsh,*[a] Noelia M. Sanchez-Ballester,[b] Valeska P. Ting,[c] Simon R. Hall,[d] Lui R. Terry,[d] and Mark T. Weller*[a]

A range of low cost nanoparticulate mixed transition metal oxides were prepared using a simple methodology and used as catalysts in visible light promoted water oxidations. The effect of catalyst and daylight equivalent light intensities on reaction efficiency in terms of O_2 yields, TOF and proton production was determined.

The capture and storage of energy in the form of convenient, inexpensive fuels remains technically elusive. The design of solar-fuel generation systems with the required efficiency, scalability, and sustainability to be economically viable has clear benefits. Artificial photosynthesis utilizes processes that encompass Photosystem II (PSII) water oxidation is a vital step towards linking with development of Photosystem I (PSI) like systems for the complete water splitting reaction and generation of liquid solar fuels.[1-3]

Water oxidation utilizes the photocycling light absorbing dye $[Ru(bpy)_3]^{2+}$, an electron acceptor quenches the excited state $[Ru(bpy)]^{2+*}$ giving $[Ru(bpy)]^{3+}$. An electron donated from a metal oxide catalyst to restores the stable $[Ru(Bpy)]^{2+}$ state and absorbed water is oxidized on the metal oxide surface with release of O_2 gas and protons.[4] In total 4 photons generate 4 protons and an O_2 molecule. The future goal is proton reduction to H_2 or simple hydrocarbon production, such as methanol, via CO_2 reductions.[5, 6]

Previously, ruthenium or iridium metal oxides or complexes have been successfully employed as the catalyst.[7, 8] Recently cobalt oxides or ligated cobalt complexes and also nickel based oxides have been shown to be effective agents.[9-13] Whilst cobalt and nickel based catalysts are less costly compared rare earth metals, these compounds are highly toxic, allergens and potent carcinogens.[14, 15] Therefore in this work we have investigated the use of lower toxicity and economic 3d transition metals as alternatives to act as catalysts for the visible light promoted water oxidation reaction. Use of these catalysts together with the effect of realistic light intensity levels on the water oxidation reaction rate, longevity and quantum yield (φ) has been investigated.

A range of spinel metal oxides were prepared using a simple combustion synthesis significantly adapted from the Pechini citric acid and glycol methodology (**Table 1**).[16] Briefly, metal nitrate salts were mixed in solution with the biopolymer dextran, ammonia solution was then added to form suspensions of the oxide. These were dried and heated very briefly to 450ºC to promote a controlled combustion to readily form low density porous frameworks that ranged in colour from brick red for iron oxide through to pure black for cobalt oxide preparations (experimental details are described in the ESI†). The frameworks were composed of loosely connected nanoparticles of the metal oxides as shown by SEM (ESI† Fig.S1). Powder XRD measurements were conducted to identify the metal oxide phases obtained. These gave quite broad reflections that corresponded to low crystalline pure phase cobalt oxide as Co_3O_4 (JCPDS 42-1467), spinel ferrite oxides of $CoFe_2O_4$ (JCPDS 02-1086) and $MnFe_2O_4$ (JCPDS 10-0139), and a mixed phase of γ-Fe_2O_3 (maghemite) (JCPDS 39-1346) and σ-Fe_2O_3 (hematite) (JCPDS 33-0664) (**Fig. 1**). A weak reflection at d(Å)3.68 corresponding to {012} facets of hematite was present, notably this crystal face has been implicated with increased water oxidation activity in photocatalysed reactions in conjunction with $[Ru(bpy)]^{2+}$ sensitizer.[17] The UV-visible absorption spectrum of this mixed phase sample was measured and a Tauc plot of (ah□□^{2}□against (h□) for the direct transition gave a band gap of ~1.98eV which corresponds to the reported value for maghemite (ESI† Fig. S2 a,b).[18]

Low crystallinity nanoparticles were obtained due to the low temperature and short heating methodology employed. Phase composition was confirmed by Raman spectroscopy of the samples (ESI† Fig. 3). The size and shape of the particles that compose the open framework structured formed from the combustion step were analyzed by TEM, this showed irregular spherical and cubic nanoparticles ranging from ~10-15nm for Co_3O_4 up to irregular faceted block shaped 30nm nanoparticles for Fe_2O_3 were formed (ESI† Fig. S4). Brunauer, Emmett and Teller (BET) surface area measurements of lightly ground samples were commensurate with the TEM observations (Table 1).

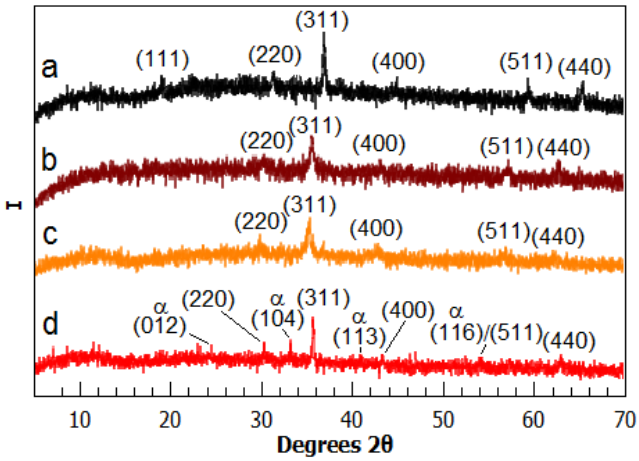

Fig. 1 Powder X-ray diffractograms of prepared metal oxides showing (a) Co_3O_4; (b) $CoFe_2O_4$; (c) $MnFe_2O_4$; (d) γ-Fe_2O_3 and α-Fe_2O_3 mixed phase.

The prepared metal oxides were employed as catalysts in visible light photocatalyzed water oxidations using $[Ru(bpy)_3]^{2+}$ light sensitizer. Persulphate has traditionally been used as an electron acceptor, however the powerful sulphate radical anion ($SO_4^{-\cdot}$) formed promotes oxidative decomposition of reagents, generation of CO_2 and shortening of reaction lifetimes.[3] $[Co(NH_3)_5Cl]Cl_2$ was used as electron acceptor, though previously it has been shown that at longer reaction times cobalt oxide can be generated in-situ which can then contribute to catalytic activity.[11, 19] Thus rate and yield obtained within 35min of light-on was used for evaluation here. Stirred reactions were conducted in N_2 degassed acetate buffer, illuminated with a 3W blue led (λmax 465nm) lamp at a specific distance from the reaction flask surface to give a measured light intensity of at the outer flask surface. Release of O_2 and reaction mixture pH were monitored simultaneously in–situ and in real time. An optical O_2 sensor combined with a temperature compensation probe was used for accurate gaseous O_2 measurements (experimental details are described in the ESI†).

$2H_2O + 4h\nu \rightarrow O_2\uparrow + 4H^+ + 4e^-$ (to buffer/ electron acceptor)

Reactions were also conducted using a commercial laser ablated sample of Co_3O_4 (Com-Co_3O_4) nanopowder as comparison. Taking the maximum O_2 yield within the initial 35 minutes of light exposure showed that the prepared and highest surface area Co_3O_4 catalyst sample gave highest yield, followed by the mixed phase Fe_2O_3. The $CoFe_2O_4$ sample, with the manganese ferrite $MnFe_2O_4$ and commercial Co_3O_4 gave the lowest yields. The highest initial Turn Over Frequency (TOF) and φ was obtained with Co_4O_4, $MnFe_2O_4$ produced the second fastest rate, which was reflected in the relatively high measured surface area of this oxide. However O_2 generation was not as sustained as with Fe_2O_3 and $CoFe_2O_4$ whose O_2 production rates were similar (**Fig. 2**). It may be that the cobalt component, in particular Co^{3+} in octahedral sites as indicated by a prominent T_{2g} Raman Shift at ~470cm^{-1} (ESI† Fig. S3c),[20] promotes activity disproportionate to the lower surface area of this sample.[21] The laser ablated commercial Co_3O_4 gave a relatively moderate O_2 yield and rate in comparison. Heterogeneous catalyst activity depends on a number of factors including surface area, metal oxidation states, surface texture and favourable facets and edges.

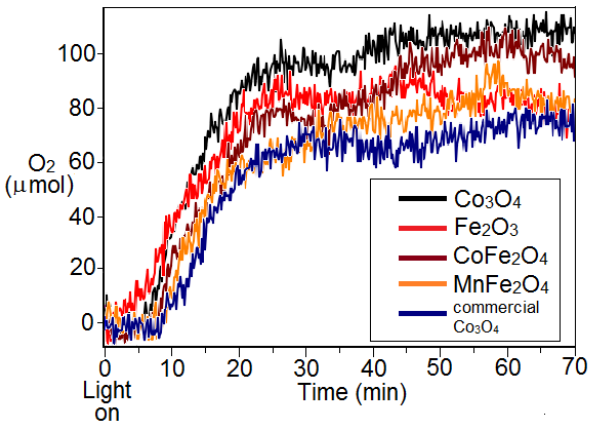

Fig. 2 Visible light photocatalysed water oxidations showing O_2 yield with time using 5 $mWcm^{-2}$ blue light with 10mg catalyst of (a) Co_3O_4; (b) γ-Fe_2O_3 and α-Fe_2O_3; (c) $CoFe_2O_4$; (d) $MnFe_2O_4$; (e) commercial Co_3O_4 nanopowder.

Table 1 Maximum net O_2 generated and production rate (from 5-15 min), calculated TOF's (TOF as mol O_2 sec^{-1}/mol (active) metal). Quantum yield $\Phi O_2\%$ = O_2 produced at t = $O_{2max\ <35min}$/photons absorbed at t= 35min × 400% (4 photons absorbed per O_2). (Example calculations are shown in the ESI†).

Sample (S_{BET} m^2g^{-1})	O_2 yield (at t<35min) □ □mol	O_2 (5-15min)/ □mol s^{-1}	TOF_{max} 10^{-3} s^{-1}	$\varphi O_2\%$ (at t= 35 min)
Co_3O_4 (61.3)	98	0.105	0.843	31.1
Fe_2O_3 (38.7)	83	0.067	0.535	25.9
$CoFe_2O_4$ (27.8)	77	0.069	0.542	24.4
$MnFe_2O_4$ (39.6)	76	0.077	0.597	24.1
Com-Co_3O_4 (35.8)	70	0.055	0.442	22.2

In some instances amorphous phases have been reported to be more effective, whilst in others crystal edges have been implicated in higher activity.[22, 23] It may be that rapid combustion with a short heating step give the low crystalline mixed phase and mixed metal oxides that are more optimal for this catalysis. The products may have more numerous surface defects, edges and interfaces between conjoined nanoparticles that favour water bonding and the subsequent oxidation reaction sequence. In the case of Fe_2O_3 several additional factors may be combining to increase O_2 yield. Firstly the presence of {012} facets,[17] also the mixed γ/α phase may allow more dynamic electronic transitions that facilitate electron transfer to the $[Ru(bpy)_3]^{3+}$ and transient Fe^{3+}-Fe^{4+}-Fe^{3+} upon oxidation of water to O_2 and protons.

Catalyst recycling

The mixed phase ferrimagnetic maghemite/ ferromagnetic hematite Fe_2O_3 catalyst responded well to a strong magnet and could be easily collected from a completed water oxidation reaction for re-use. O_2 evolution profiles from four successive reactions using recovered Fe_2O_3 as the catalyst were measured (**Fig. 3**). This showed that the most rapid onset of O_2 generation occurred on initial use, thereafter an increasing lag was present. O_2 yields were similar for the first three successive reactions, with a moderate decrease evident upon fourth use. The recovered and washed Fe_2O_3 catalyst darkened with successive usage (ESI† Fig. S5). TEM of the sample showed the Fe_2O_3 crystals had become decorated with nanoparticles.

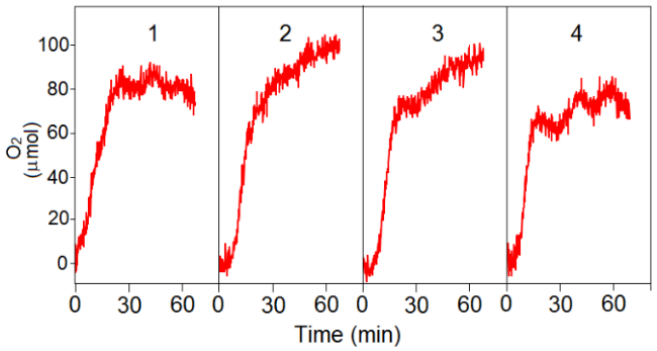

Fig. 3 Visible light photocatalysed water oxidations showing O_2 yield with time using 5 mWcm^{-2} blue light with 10mg catalyst of mixed phase Fe_2O_3 which was recovered and re-used in a further three successive reactions.

XRD showed the presence of a low level of Co_3O_4/ $Co(OH)_x$ suggesting that the accumulated surface material was nanoparticles of cobalt oxide derived from decomposed electron acceptor (ESI† Fig. S6a,b). Accumulation of the cobalt oxide may account for increased lag times and fluctuations in O_2 output in successive reactions after the initial 25-30 min linear phase, due to complex interplay between cobalt oxidized to Co_3O_4 producing high catalytic activity coupled with electron extraction from excited state $Ru(bpy)^{2+*}$ being diverted to oxidation of cobalt hydroxide into Co_3O_4 without O_2 generation.

Light intensity

For practical application of this approach to solar fuel production it should be able to operate at natural daylight intensities, including on overcast days and in locations at higher latitude with varying annual day length and lesser light intensity compared to equatorial regions. Our measurements have shown that (at~51°N and 170m elevation) in direct sunlight at noon the 420-490nm light intensity varies between 5 mWcm^{-2} in December, to 9 mWcm^{-2} at spring and autumn equinox's to reach a maximum of 10.5 mWcm-^{2} in June (**Fig. 4**).

The quality of light varies greatly on overcast days however, being upwards from a minimum of ~0.5 mWcm^{-2}. Therefore the effect of incoming light intensity on the water oxidation reaction was investigated. As the mixed phase Fe_2O_3 is relatively non-toxic, highly abundant and performed well in the water oxidations it was used as the metal oxide catalyst. Recently it been reported that more complex molecular iron based water oxidation catalysts convert to Fe_2O_3 within the reaction which then can act as the actual catalyst.[24] A series of water oxidation reactions was conducted using matching reaction reagents and protocol except that the blue led light impinging on the reaction flask was set to generate values ranging between 0.6 – 10 mWcm^{-2} as a match to realistic daylight levels.

Fig. 5a shows O_2 release profiles under increasing light intensity. O_2 yields and TOF were shown to be dependent on light intensity, with 10 mWcm^{-2} producing a maximum O_2 yield of 118 µmol O_2, close to the maximum theoretical 120 µmol yield based on electron acceptor concentration.5 mWcm^{-2} light gave rate and O_2 output intermediate between the 10 and 2.5 mWcm^{-2} values. Only a marginal reduction was obtained between 2.5 to 1.3 mWcm^{-2}. Lag between light-on and onset of O_2 and proton production was seen to lengthen as light intensity was lowered. Thereafter photocycling appeared to be less dependent on light intensity as reaction rates were similar. When light intensity was lowered to 0.6 mWcm^{-2} a prolonged lag phase of over 20 min. before onset of minimal activity

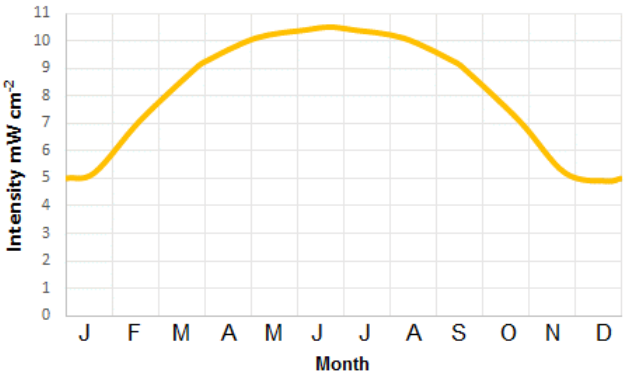

Fig. 4 Measured monthly maximum light intensity (over 420-490nm with clear sky at noon at 51.4°N latitude and 170m elevation)

was found, this light intensity appears to fall below the minimum level for satisfactory cyclic photocatalyzed oxidation.

The more rapid onset of O_2 production at both 10 and 5 $mWcm^{-2}$ suggests that initially the higher intensity is required for full light saturation of the $[Ru(bpy)3]^{2+}$ sensitizer (**Table 2**). At lower light levels the delay indicates a build-up in concentration of the excited state $[Ru(bpy)_3]^{2+*}$ was required before onset of water oxidation.

At higher light intensity an abrupt cessation of water oxidation appears to occur after 20-25 min, this was most likely caused by exhaustion of the electron acceptor and at 10 mW also onset of decomposition of the $[Ru(bpy)_3]^{2+/3+}$ due to elevated pH. With this Fe_2O_3 sample the rapid pH rise and absence of a second stage of O_2 evolution at longer timescale suggests that Co_3O_4 generated by oxidation of $Co(OH)_x$ from the decomposed electron acceptor contributed to O_2 production to this single O_2 generation phase observed.[19] Samples reacted using light intensity between 5-1.3 mW showed a minor upswing in O_2 production from ~40min onwards, indicating that onset of activity of in-situ formed Co_3O_4 occurred at around this point.

Fig. 5b shows the corresponding change in pH with time, reduction of the pentamine cobalt electron acceptor and release of ammonia results in the increase in pH of the buffered solution as water oxidation proceeded. An inflexion point marked the onset of O_2 release after between approximately 5 – 20 minutes depending on light intensity. Here a burst of proton and O_2 production appeared to occur which resulted in a transient levelling off of pH rise.

Table 2 Effect of light intensity on maximum net O_2 generated and production rate (from 5-15 min), calculated TOF's (TOF as mol O_2 sec^{-1}/mol Fe). Quantum yield $\Phi O_2\%$ = O_2 produced at t = $O_{2max\ <35min}$/photons absorbed at t= 35min × 400% (4 photons absorbed per O_2). 10mg of mixed phase Fe_2O_3 used as catalyst in each reaction.

γ/α-Fe_2O_3 Light intensity ($mW\ cm^{-2}$)	O_2 yield (at t<35min) µmol	O_2 (5-15min)/ µmol s^{-1}	TOFmax 10-3 s^{-1}	$\varphi O_2\%$ (at t= 35 min)
10	117	0.144	1.153	18.5
5	83	0.067	0.535	25.9
2.5	80	0.055	0.443	50.8
1.3	76	0.03	0.24	92
0.6	8	-	-	24.5

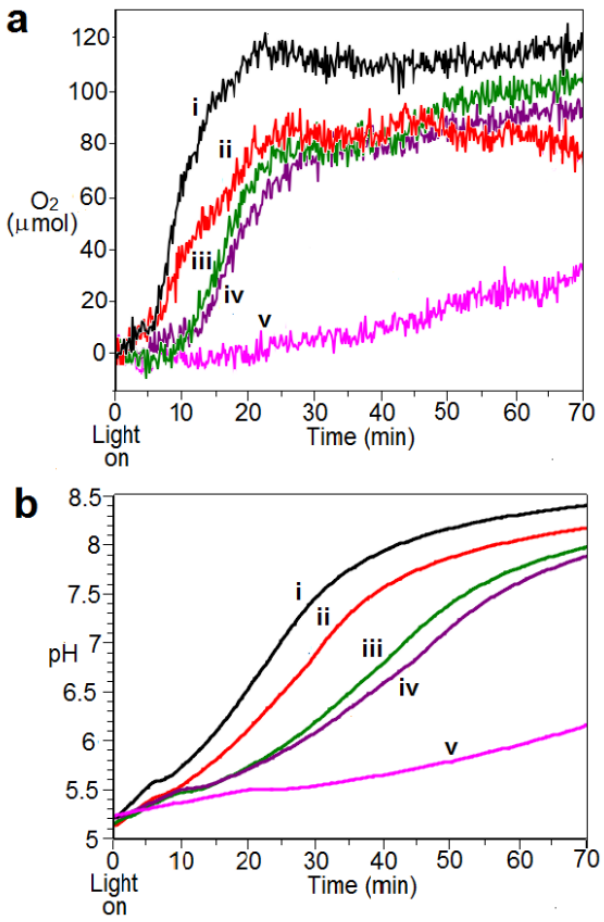

Fig. 5 (a) photocatalysed water oxidation showing O_2 yield with time using 10mg of prepared mixed phase Fe_2O_3 catalyst and (b) change in pH with time. Blue light intensity ($mWcm^{-2}$) of (i) 10; (ii) 5; (iii) 2.5; (iv) 1.3; (v) 0.6.

Conclusions

A simple methodology was devised using minimal energy input for the synthesis of functional metal oxide nanoparticles. The prepared catalysts low crystallinity with accessible and abundant edges may have contributed to their activity. Cobalt oxide as Co_3O_4 was found to be most effective in terms of O_2 yield and TOF for the photocatalyzed water oxidations, however a mixed phase Fe_2O_3, which is more desirable in terms of toxicity, was almost as effective. This catalyst was shown to be readily collected for re-use, though gradual accumulation of surface bound nanoparticles of cobalt oxide from decomposed electron acceptor occurred. Reactions were conducted using light intensities that realistically match daylight levels, as opposed to very high intensity sources that have commonly been employed previously. The results showed that the water oxidation reaction successfully occurred, though with increase in lag time, down to 1.3 $mWcm^{-2}$. The optimum light intensity in terms of O_2 yield and proton production rate, whilst minimising side reactions of decomposition of light sensitizer and re-organization of the electron acceptor into a catalyst, appeared to be around 5 $mWcm^{-2}$. A marked drop in reaction occurred between 1.3 to 0.6 $mWcm^{-2}$, the lowest light level appeared to be below the threshold for sufficient build-up of the excited state $Ru(bpy)_3^{2+*}$ with only a very minimal water oxidation reaction and O_2 yield resulting.

Further studies on surface topology of prepared materials and replacing the electron acceptor with a reversible electron storage mediator as a step towards solar fuel production are currently underway.

Notes and references

DW and MTW acknowledge funding by a UoB Faculty of Science departmental grant. VPT acknowledges funding from a UoB Prize Research Fellowship. SRH and LRT acknowledges the USAF European Office of Aerospace Research and Development (FA8655-12-1-2078).
ESI† : Experimental details, SEM, Raman analysis, UV-vis spectroscopy, TEM, XRD, example calculations.

1. S. Styring, *Faraday Discussions*, 2012, **155**, 357-376.
2. Y. Tachibana, L. Vayssieres and J. R. Durrant, *Nat Photon*, 2012, **6**, 511-518.
3. K. J. Young, L. A. Martini, R. L. Milot, R. C. Snoeberger Iii, V. S. Batista, C. A. Schmuttenmaer, R. H. Crabtree and G. W. Brudvig, *Coordination Chemistry Reviews*, 2012, **256**, 2503-2520.
4. A. Harriman, G. Porter and P. Walters, *Journal of the Chemical Society, Faraday Transactions 2: Molecular and Chemical Physics*, 1981, **77**, 2373-2383.
5. C. Herrero, A. Quaranta, W. Leibl, A. W. Rutherford and A. Aukauloo, *Energy & Environmental Science*, 2011, **4**, 2353-2365.
6. M. Morikawa, Y. Ogura, N. Ahmed, S. Kawamura, G. Mikami, S. Okamoto and Y. Izumi, *Catalysis Science & Technology*, 2014, **4**, 1644-1651.
7. L. L. Duan, Y. H. Xu, P. Zhang, M. Wang and L. C. Sun, *Inorg. Chem.*, 2010, **49**, 209-215.
8. N. D. Morris, M. Suzuki and T. E. Mallouk, *J. Phys. Chem. A*, 2004, **108**, 9115-9119.
9. F. Jiao and H. Frei, *Angew. Chem.-Int. Edit.*, 2009, **48**, 1841-1844.
10. D. Shevchenko, M. F. Anderlund, A. Thapper and S. Styring, *Energy & Environmental Science*, 2011, **4**, 1284-1287.
11. D. Hong, J. Jung, J. Park, Y. Yamada, T. Suenobu, Y. M. Lee, W. Nam and S. Fukuzumi, *Energy & Environmental Science*, 2012, **5**, 7606-7616.
12. D. Hong, Y. Yamada, T. Nagatomi, Y. Takai and S. Fukuzumi, *Journal of the American Chemical Society*, 2012, **134**, 19572-19575.
13. P. W. Menezes, A. Indra, O. Levy, K. Kailasam, V. Gutkin, J. Pfrommer and M. Driess, *Chemical Communications*, 2015, **51**, 5005-5008.
14. D. Lison, M. De Boeck, V. Verougstraete and M. Kirsch-Volders, *Occupational and Environmental Medicine*, 2001, **58**, 619-625.
15. L. J. Smith, A. L. Holmes, S. K. Kandpal, M. D. Mason, T. Zheng and J. P. Wise Sr, *Toxicology and Applied Pharmacology*, 2014, **278**, 259-265.
16. *United States Pat.,* 3330697, 1967.
17. Q. Xiang, G. Chen and T.-C. Lau, *RSC Advances*, 2015, **5**, 52210-52216.
18. M. I. Litter and M. A. Blesa, *Canadian Journal of Chemistry*, 1992, **70**, 2502-2510.
19. D. Walsh, N. M. Sanchez-Ballester, K. Ariga, A. Tanaka and M. Weller, *Green Chemistry*, 2015, **17**, 982-990.
20. P. Chandramohan, M. P. Srinivasan, S. Velmurugan and S. V. Narasimhan, *Journal of Solid State Chemistry*, 2011, **184**, 89-96.
21. A. Indra, P. W. Menezes, N. R. Sahraie, A. Bergmann, C. Das, M. Tallarida, D. Schmeißer, P. Strasser and M. Driess, *Journal of the American Chemical Society*, 2014, **136**, 17530-17536.
22. M. M. Najafpour, S. Nayeri and B. Pashaei, *Dalton Transactions*, 2011, **40**, 9374-9378.
23. B. Barrocas, S. Sério and M. E. Melo Jorge, *The Journal of Physical Chemistry C*, 2014, **118**, 24127-24135.
24. G. Chen, L. Chen, S.-M. Ng, W.-L. Man and T.-C. Lau, *Angewandte Chemie International Edition*, 2013, **52**, 1789-1791.